Available online at www.sciencedirect.com
SCIENCE DIRECT
Polymer 46 (2005) 10301–10310
polymer
www.elsevier.com/locate/polymer

Nematic-like mesophase photoconductive polymer for photorefractive applications

O-Pil Kwon[a,*], Seong-Ji Kwon[a,b], Mojca Jazbinsek[a], Suck-Hyun Lee[b], Peter Günter[a]

[a]*Nonlinear Optics Laboratory, Institute of Quantum Electronics, Swiss Federal Institute of Technology, ETH Honggerberg, CH-8093 Zurich, Switzerland*
[b]*Department of Molecular Science and Technology, Ajou University, Suwon 442-749, South Korea*

Received 28 January 2005; received in revised form 20 July 2005; accepted 29 July 2005
Available online 19 August 2005

Abstract

A new nematic-like mesophase photoconductive polymer PPT–TPA consisting of wholly aromatic rigid backbone of poly(*p*-phenyleneterephthalate), PPT and pendent hole-transporting triphenylamine (TPA) groups attached to the ends of oxydecyl spacers has been synthesized. The photorefractive composite contains the photoconductor PPT–TPA, the chromophore diethylaminodicyanostyrene (DDCST), and the photosensitizer C_{60}. Although no plasticizer was added, the glass transition temperature T_g of the composite is 15 °C, which characterizes it as a low-T_g photorefractive material. We investigate the correlation between the mesophase structure and its optical/physical properties by X-ray diffraction, photoconductive and photorefractive experiments. The new composite and its properties are compared to PPT–CZ composites with only a different charge transporting agent (carbazole, CZ) but a much more ordered mesophase structure, which were studied previously and have shown very good photorefractive properties. Despite of a lower photoconductivity of the new photorefractive composite PPT–TPA ($n=10$):DDCST:C_{60} this material shows a higher photorefractive sensitivity S_{n2} of 2 ± 0.2 cm^2/kJ at $E=50$ V/μm than the previously synthesized composite PPT–CZ ($n=10$):DDCST:C_{60}.

Keywords: Photorefractive materials; Photoconductive materials; Photorefractive nonlinear optics

1. Introduction

Rigid-rod polymers with flexible side chains have been studied extensively for the last two decades since the discovery of their self-organized layered structures [1–12]. An introduction of flexible side chains to a wholly aromatic rod-like polymer backbone leads to layered mesophase structures, where the flexible side chains occupy the space between the layers formed by the main chains. The layer structured aromatic polymers have lower melting points and greater solubility than simple aromatic polyesters without side chain groups [1–7]. Most efforts have been devoted towards a better understanding of the structural phase behavior and mechanical properties in relation to the chemical structures with long alkyl side chains.

A few reports have discussed the correlation between the phase behavior and the chemical/physical properties for the layer-structured polymers with functionalized side groups such as nonlinear optical (NLO) active chromophores [8,9], photoconducting groups [10], and other functional groups [13] instead of the long alkyl side chains without functional groups. In the past few years, we have reported the NLO properties of side group polymers based on a rigid backbone, poly(*p*-phenylene terephthalate), PPT [9,14–17]. We observed considerably different phase behavior depending on the linking structure of the chromophores, when similar NLO chromophores were attached as side groups to the same backbone [9].

Polymeric photorefractive materials, first reported in 1991 [18], have been of particular interest [19–23] due to their numerous potential applications such as high-density optical data storage, optical image processing, and phase conjugation mirror [24]. The photorefractive effect involves the modulation of the refractive index by a photoinduced space charge field [24]. Photorefractive materials require both good photoconductive and electro-optic properties [25]. The carbazole (CZ) and triphenylamine (TPA) derivatives have been widely used as the charge transporting

* Corresponding author. Tel.: +41 1 633 3258; fax: +41 1 633 1056.
E-mail address: kwon@phys.ethz.ch (O.-P. Kwon).

0032-3861/$ - see front matter © 2005 Elsevier Ltd. All rights reserved.
doi:10.1016/j.polymer.2005.07.104

agents in organic photoconductors [26–29]. In a recent work, we have introduced photoconductive groups into the layer structured polymer in order to enhance the photorefractive effect by the quadratic orientational effect [21] and increase the thermal stability without phase separation problems [10–12]. The photorefractive properties of the polymer composites based on a layered photoconducting polymer PPT–CZ employing a PPT rigid backbone and pendent carbazole (CZ) groups have been investigated (Scheme 1). They showed a layered mesophase structure even though the bulky carbazole groups at the ends of the alkyl spacers can interfere with layering. The PPT–CZ composites were shown to exhibit excellent photorefractive properties. A two-wave mixing gain coefficient up to $\Gamma \approx 250\ \mathrm{cm}^{-1}$ at an applied electric field $E = 60$ V/μm and a photorefractive sensitivity $S_{n2} \approx 70\ \mathrm{cm}^2/\mathrm{kJ}$ at $E = 100$ V/μm were observed [10–12].

To extend our previous study a new photoconductive polymer PPT–TPA was designed and synthesized by replacing the photoconductive groups in the PPT–CZ polymers with triphenylamine (TPA) groups in order to improve the charge carrier transport (Scheme 1). This paper discusses the correlations between the mesophase structure and the optical/physical properties for PPT–TPA, also in comparison to PPT–CZ that was investigated in Ref. [10]. In order to clearly confirm the influence of different photoconducting groups for the mesophase structure, the PPT–TPA composite was compared to a PPT–CZ composite with the same weight ratio of the photorefractive ingredients, with the same NLO chromophore and sensitizer, and the same length of alkyl spacer ($n = 10$) in the photoconducting polymer. These polymers were characterized by differential scanning calorimetry (DSC), X-ray diffractometry, photoconductivity, photorefractive two-beam coupling, and Bragg diffraction measurements.

2. Experimental

2.1. Materials

All chemicals were obtained from commercial suppliers and used as received unless otherwise noted. Tetrahydrofuran (THF) was distilled over sodium and benzophenone. All reactions were carried out under a nitrogen atmosphere unless otherwise noted.

2.2. General characterization

^{1}H NMR spectra were recorded on a Varian 400. The chemical shifts are reported in ppm (δ) relative to $(CH_3)_4Si$. IR spectra were recorded on a Nicolet 800 Fourier transform infrared spectrometer. UV–vis absorption spectra were recorded on a Jasco V-570 UV/vis/NIR spectrophotometer. Thermal measurements were carried out using a Diamoind DSC from Perkin–Elmer in the differential scanning calorimetry and TGA-50 systems from TA instruments in the thermogravimetry (10 K/min scan rate). Wide angle X-ray diffraction studies were performed using a GADDS (Bruckr Co.).

2.3. Synthesis of monomers

The synthesis route of the monomer (TPA10-acid, **5**) for polymer PPT–TPA ($n = 10$) is shown in Scheme 2. *N*-(4-formylphenyl) diphenylamine (TPA-CHO, **1**) and *N*-(4-hydroxymethylphenyl) diphenylamine (TPA-CH_2OH, **2**) were synthesized according to the literature [30].

2.3.1. 1-[4-[N-(diphenylamino)phenyl]methoxy]-10-bromodecane (TPA10-Br, *3*)

TPA-CH_2OH (**2**, 44 mmol, 12.22 g) and 1,10-dibromodecane (132 mmol, 29.77 mL) were dissolved in THF (100 mL). To this mixture we added a 60% dispersion of sodium hydride in mineral oil (132 mmol, 5.3 g) over 1 h period. The resulting mixture was stirred for 24 h at 60–65 °C and filtered. The filtrate was concentrated in vacuum and then separated by column chromatography (EtOAc/*n*-Hexane = 1/20). TPA10-Br (19.0 g) was obtained as a yellow viscous liquid in 87% yield. ^{1}H NMR ($CDCl_3$): δ_H 1.2–1.5 (m, 12H, –CH_2–), 1.6 (m, 2H, –CH_2–), 1.8 (m, 2H, –CH_2–), 3.4 (t, 2H, –CH_2Br), 3.5 (t, 2H, –OCH_2–), 4.4 (s, 2H, ArCH_2–), 6.9–7.3 (m, 14H, aromatic protons). IR (NaCl), cm^{-1}: 3100–3000 (aromatic C–H), 2960–2840 (aliphatic C–H), 1350–1000 (C–N), 750, 700 (aromatic OOP).

2.3.2. Diethyl 2,5-di-[1-[4-[N-(diphenylamino)phenyl]methoxy]decyleneoxy]terephthalate (TPA10-ester, *4*)

Diethyl 2,5-dihydroxy terephthalate (8.3 mmol, 2.12 g) and K_2CO_3 (25.0 mmol, 3.46 g) were dissolved in dry DMF (60 mL). To this solution we added TPA10-Br (**3**, 19.2 mmol, 9.50 g) in DMF, and the mixture was stirred at 60 °C for 40 h. The resulting mixture was filtered to

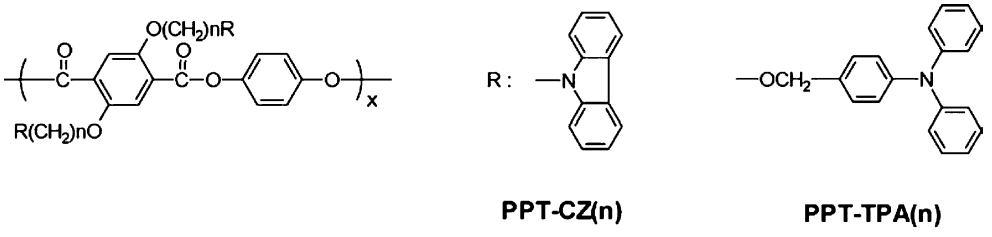

PPT-CZ(n) PPT-TPA(n)

Scheme 1. Chemical structures of the investigated polymers.

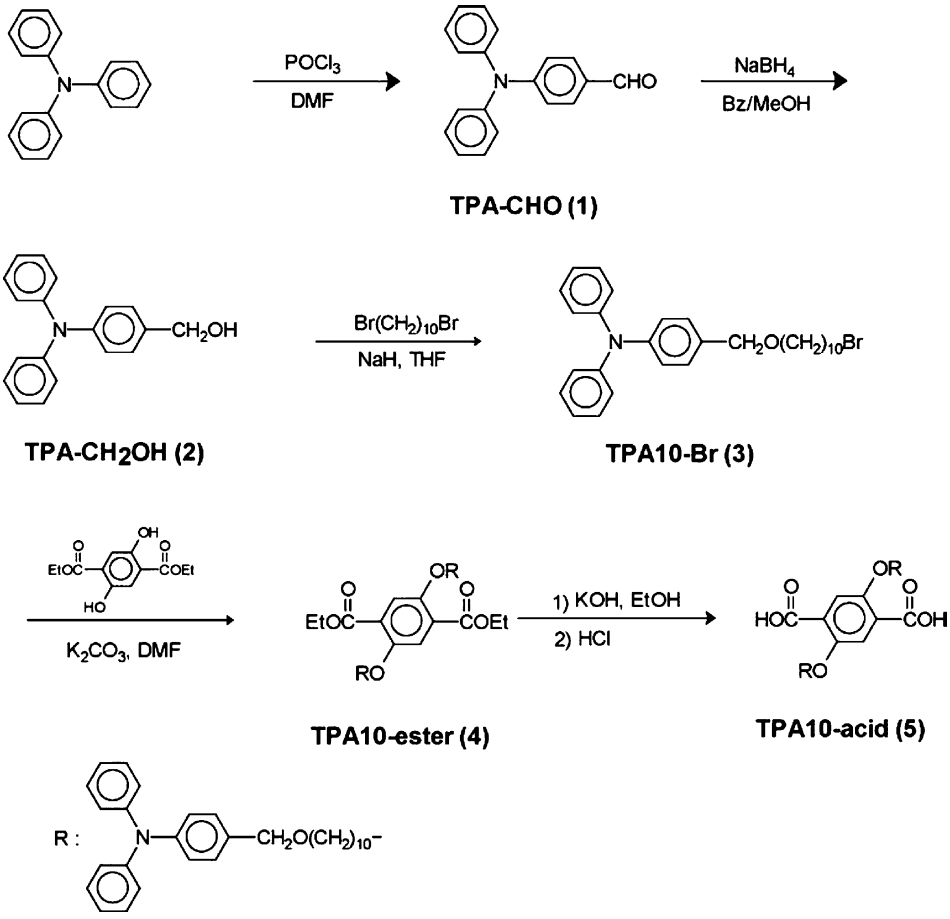

Scheme 2. Synthesis of the TPA10-acid monomer.

remove K_2CO_3, and then DMF was removed by the vacuum distillation. The concentrate was separated by column chromatography (EtOAc/*n*-Hexane = 1/10) to give a yellow viscous liquid (6.8 g, 76%). ^{1}H NMR ($CDCl_3$): δ_H 1.2–1.5 (m, 30H, –CH_2– and –CH_3), 1.6 (m, 4H, –CH_2–), 1.8 (m, 4H, –CH_2–), 3.5 (t, 4H, –OCH_2–), 4.0 (t, 4H, –OCH_2–), 4.37 (q, 4H, ArO–CH_2–), 4.4 (s, 4H, ArCH_2–), 6.8–7.2 (m, 28H, aromatic protons), 7.3 (2H, Ar–H from terephthalate). IR (NaCl), cm^{-1}: 3100–3000 (aromatic C–H), 2960–2840 (aliphatic C–H), 1730 (C=O), 1350–1000 (C–N), 750, 700 (aromatic OOP).

2.3.3. 2,5-Di-[1-[4-[N-(diphenylamino)phenyl]methoxy] decyleneoxy]terephthalic acid (TPA10-acid, **5**)

TPA10-ester (**4**, 5.3 mmol, 5.73 g) was added in ethanol (250 mL) and then dissolved under reflux. To this solution we added KOH (21.2 mmol, 1.9 g). After the reaction was terminated, the reaction mixture was concentrated in vacuum to give a yellow powder. Water was added to this powder, and then treated with 2N–HCl until pH 2–3. This mixture was extracted with methylene chloride (3× 300 mL). The organic phases were dried over sodium sulfate and evaporated in vacuum to give a yellow solid. This was purified by recrystallization in methanol to give the product (5.4 g, 90%). ^{1}H NMR ($CDCl_3$): δ_H 1.2–1.5 (m, 24H, –CH_2–), 1.6 (m, 4H, –CH_2–), 1.9 (m, 4H, –CH_2–), 3.5 (t, 4H, –OCH_2–), 4.3 (t, 4H, ArO–CH_2–), 4.42 (s, 4H, ArCH_2–), 6.8–7.2 (m, 28H, aromatic protons), 7.85 (2H, Ar–H from terephthalic acid), 11.15 (s, 2H, –CO_2H). IR (KBr), cm^{-1}: 3600–2400 (–OH), 3100–3000 (aromatic C–H), 2960–2840 (aliphatic C–H), 1740 (C=O), 1350–1000 (C–N), 750, 700 (aromatic OOP).

2.4. Polymerization

The 2,5-disubstituted terephthalic acid, TPA10-acid (**5**) was polymerized by solution condensation polymerization with hydroquinone [31]. PPT–TPA (n = 10): TPA10-acid (**5**, 0.925 g, 0.88 mmol) was dissolved in dry pyridine (30 mL). A solution was treated with diphenyl chlorophospate (DPCP) (0.47 mL, 2.28 mmol) at room temperature for 30 min, and then with LiCl for 30 min, and the mixture was maintained at 90 °C for 60 min to give a red-colored solution. To this solution hydroquinone (0.097 g, 0.88 mmol) in pyridine (10 mL) was dropwised and the resulting solution was maintained at 90 °C for 40 min. After the reaction was terminated, the reaction mixture was poured into methanol and the precipitated polymer was

separated by filtration and washed well with methanol and water. The obtained polymer was dried in vacuum oven at 50 °C. ^{1}H NMR ($CDCl_3$): δ_H 1.2–1.5 (m, 24H, –CH_2–), 1.6 (m, 4H, –CH_2–), 1.9 (m, 4H, –CH_2–), 3.5 (t, 4H, –OCH_2–), 4.1 (s, 4H, ArO–CH_2–), 4.4 (s, 4H, ArCH_2–), 6.8–7.4 (m, 32H, aromatic protons), 7.6 (2H, s, Ar–H from terephthalate), IR (KBr), cm^{-1}: 3100–3000 (aromatic C–H), 2960–2840 (aliphatic C–H), 1750 (C=O), 1350–1000 (C–N), 750, 700 (aromatic OOP).

2.5. Photorefractive sample preparation

The photorefractive composites consisted of the mesophase photoconductive polymer PPT–TPA ($n=10$) (64.5 wt%), the chromophore diethylaminodicyanostyrene (DDCST) (35 wt%), and the sensitizer C_{60} (0.5 wt%). No plasticizers were added. These ingredients were dissolved in 1,1,2,2,-tetrachloroethane (TCE) and the solution was filtered with a teflon membrain filter (Milipore, 0.45 μm). The film specimen was cast onto the indium-tinoxide (ITO) coated glass slides from the TCE solution, and then the solvent was evaporated during 2 h at 120 °C. The film sample was finally assembled using teflon spacers of 100 μm thickness to ensure a uniform sample thickness at a temperature around 160 °C.

2.6. Photoconductive properties

The dc photoconductivity of photorefractive composites has been determined by measuring the current flow through the samples during illumination with a He–Ne laser beam ($\lambda=633$ nm) by varying the electric field and the laser intensity.

2.7. Electro-optic properties

The effective linear electro-optic coefficients were determined from the field-induced birefringence measurements by using a Babinet–Soleil compensator. A He–Ne laser beam ($\lambda=633$ nm) was incident at an external angle of 50° with respect to the sample normal. Its polarization was set to $+45°$ with respect to the propagation plane, and the transmitted light was probed through a $-45°$ analyzer. A compensator was placed between the sample and the analyzer and adjusted so that the analyzer blocked all the transmitted light. The phase shift was determined by $\Delta\phi=\Delta x/\Delta x_{360°}$, where Δx is the length for which the compensator was moved from the position with the minimum transmission without the sample, and $\Delta x_{360°}$ is the length for which the compensator was moved between the two adjacent positions having minimum intensity of the transmitted light. The change of the refractive index Δn was calculated from the measured phase shift, which is given by $\Delta\phi=(2\pi/\lambda)(\Delta n\ (d/\cos\theta_{int}))$, where θ_{int} is the internal angle of the beam with respect to the surface normal.

2.8. Photorefractive properties

The photorefractive properties of the photorefractive composite were evaluated by two-beam coupling and Bragg diffraction experiments. We used a set-up similar to the one described in Ref. [10].

2.8.1. Two-beam coupling

Two-beam coupling experiments were performed at a wavelength of 633 nm (He–Ne laser). Two p-polarized beams intersected the sample in a tilted geometry configuration. The beams were of different intensities to reduce the beam fanning effect ($I_{pump}=26.0$ mW/cm^2, $I_{signal}=0.02$ mW/cm^2). The normal of the sample surface was tilted for $\Psi=45°$ with respect to the bisector of the beams, and the angle between the beams outside the sample was $2\theta_{ext}=20°$. The two beam coupling gain coefficient Γ is given by [24]

$$\Gamma=\frac{1}{d}[\ln(\gamma_0\beta_0)-\ln(\beta_0+1-\gamma_0)]$$

where $\beta_0=I_{pump}/I_{signal}$ is the intensity ratio of the two writing beams at the entrance of the sample, and $\gamma_0=I_{signal\ with\ pump}/I_{signal\ without\ pump}$. Note that in the undepleted pump regime ($\beta_0\gg1$) valid in our case the gain simplifies to $\Gamma=(1/d)\ln\gamma_0$.

2.8.2. Bragg diffraction

Photorefractive gratings were written by the illumination of two p-polarized beams from a He–Ne laser ($\lambda=633$ nm) with intensities of 29.0 and 26.0 mW/cm^2, respectively. As in the two-beam coupling experiment, the angle between the beams outside the sample was $2\theta_{ext}=20°$ and the tilt angle between the sample normal and the bisector of the beams was $\Psi=45°$. The read-out beam ($\lambda=785$ nm, 9.47 mW/cm^2) from an external cavity diode laser (crystalaser) was adjusted to the Bragg angle. Both p- and s-polarization of the read-out beam were tested. The diffraction efficiency η is calculated as the ratio of the intensities of the diffracted beam to the probe beam that is transmitted when no grating is being written in the sample by the writing beams.

3. Results and discussion

3.1. Synthesis and characterization

The synthetic routes for the preparation of the monomer, TPA10-acid (**5**) are depicted in Scheme 2. A wholly aromatic polyester PPT–TPA ($n=10$) has been prepared by the direct solution condensation of 2,5-disubstituted terephthalic acid containing the photoconducting TPA groups with hydroquinone. The direct polycondensation reaction of diphenyl chlorophosphate (DPCP) as a condensing agent in pyridine was used for the preparation of

aromatic polyesters with high molecular weight in mild condition without thionylchroride ($SOCl_2$) that is general agent to form diacid dichloride for general polycondensation reaction [31]. The chemical structures of all intermediate compounds and the polymer were confirmed by NMR and IR results.

The synthesized polymer consisted of rigid backbone poly(*p*-phenyleneterephthalate), PPT and pendent triphenylamine (TPA) groups attached at the ends of oxydecyl spacers. Note that the alkyl spacer of ten methylene units ($n=10$) was chosen here for the reason that the changes of the length of alkyl chain resulted in large changes of the photorefractive response of the previously studied PPT–CZ composites [10–12]. The PPT–CZ polymers with the spacer length longer than 8 methylenes ($n>8$) exhibited a glass transition temperture T_g near room temperature, higher solubility, and high layering ability compared to the polymers with shorter length of alkyl spacers.

We obtained the suitable molecular weight of the PPT–TPA ($n=10$) polymer by changing the reaction conditions such as temperature, time, amount of solvent. In the case of PPT–CZ the layering ability started to decrease at a certain molecular weight. Therefore, similar behavior can be expected also for PPT–TPA. Details will be reported elsewhere. Inherent viscosity was measured at a concentration of 0.1 g/dl in 1,1,2,2-tetrachloroethane (TCE). The PPT–TPA ($n=10$) polymers had the values in the range from 0.4 to 0.9 indicating that their molecular weights are suitable for well-ordered mesophase structures.

3.2. Linear optical properties

Absorption spectra of the photoconductive polymer PPT–TPA ($n=10$) are presented in Fig. 1. The absorption at ~303 nm is due to the photoconductive TPA unit and that at ~355 nm is due to the polymer backbone, poly(*p*-phenyleneterephthalate) (PPT) which is close to the absorption maximum of PPT–C ($n=10$) having the same backbone in TCE solution. The absorption peak of TPA group in the spin-coated film (dashed line) shows a slight red shift of 5 nm and is narrower than in the TCE solution (solid line). Moreover, the absorption intensity at ~355 nm connected to the PPT backbone is stronger in the film than in the solution. This behavior implies the existence of electronic interactions involving π-electrons between the side TPA group having π-electron rich phenyl groups and the polymer backbone [13]. Therefore, it is likely that the main chain and TPA groups have formed a certain ordered structure in the solid state of PPT–TPA which was further investigated by the X-ray measurements.

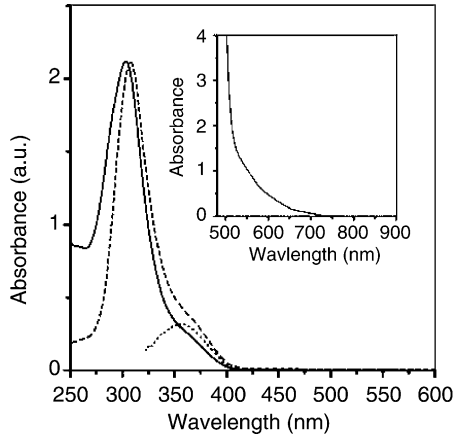

Fig. 1. Absorption spectra of the photoconductive polymer PPT–TPA ($n=10$): Solution in TCE (solid line), spin-coated film (dashed line), PPT–C ($n=10$) having same backbone and alkyl spacers without photoconducting group in dilute solution (dotted line). The Inset shows the absorbance of a 100 μm thick film of the photorefractive composite, PPT–TPA ($n=10$):DDCST:C_{60}.

3.3. Thermal properties

Thermogravimetry analysis (TGA) measurements showed that the polymer, PPT–TPA ($n=10$) has a decomposition temperature at about 315 °C (scan rate: 10 °C/min), which represents a 5% weight loss of the samples under nitrogen atmosphere.

The glass transition of the polymer measured by differential scanning calorimetry (scan rate: 10 °C/min) is near 20 °C as shown in Fig. 2. The glass transition temperature T_g is defined here as the starting point of the endotherms and is associated with the β transition of the side groups. The conventional character of the α transition of the polymer backbone is represented as a broad peak around 110 °C [9,10]. Thus, we were able to use the photoconducting host poymer PPT–TPA ($n=10$) as a low T_g photorefractive composite without the additional plasticizer.

As shown Fig. 2, the measurement of the glass transition temperature T_g of the photorefractive composite PPT–TPA ($n=10$):DDCST:C_{60} revealed a low value of about 15 °C, which classify this composite as a low-T_g material. This is an important factor for achieving high photorefractive

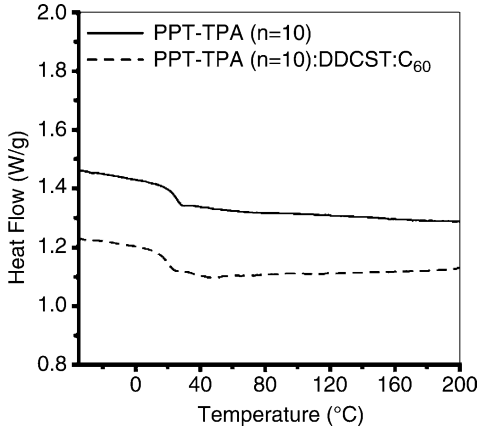

Fig. 2. DSC thermograms of the PPT–TPA polymer (solid line) and the PPT–TPA ($n=10$):DDCST:C_{60} photorefractive composite (dashed line).

performance exploiting the quadratic orientational mechanism to induce the refractive index modulation.

3.4. Mesophase structures

The intensity distributions of the X-ray diffraction of the photoconductive polymers and photorefractive composite samples prepared from the solution casting films are shown in Fig. 3. In the small diffraction angle region, PPT–TPA ($n=10$) revealed a small and a broad peak corresponding to a spacing of 24.1 and 13.2 Å, whereas PPT–CZ ($n=10$) shows two sharp peaks with a spacing of 23.3 and 11.9 Å, respectively. A stronger broad arcs with a spacing of approximately 4.3 Å were observed in the wide angle region of PPT–TPA ($n=10$). Therefore, the mesophase of PPT–TPA ($n=10$) has no long-range translational order, which is a characteristic feature of nematic mesophase, whereas PPT–CZ ($n=10$) exhibits a layered mesophase. However, we could not conclude that the structure of PPT–TPA ($n=10$) is an ordinary nematic phase by X-ray diffraction experiment because the spacing of 23.3 Å in the small angle region is too large to correspond to the ordinary nematic mesophase. Similar phenomena have been observed for polyester of pyromellitic acid and polyamide, and two possible nematic structures were suggested [4,32]. Two possible mesophases for PPT–TPA ($n=10$) are illustrated, still not fully identified, in Fig. 4(a) and (b). The layered mesophase of PPT–CZ polymer is shown in Fig. 4(c).

The reason for the different mesophases of the two polymers with the same backbone, the same length of alkyl chain and with different photoconducting groups might be related to the following two effects. First, triphenylamine groups at the ends of alkyl chains strongly influence the π-electronic interaction with the polymer backbone as

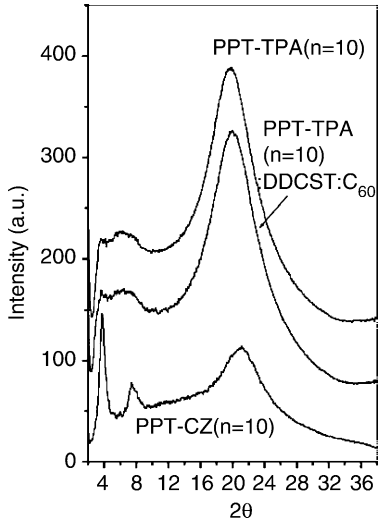

Fig. 3. X-ray diffraction patterns of the solution casting films of mesophase polymers at room temperature: From top to bottom, PPT–TPA ($n=10$), photorefractive composite PPT–TPA ($n=10$):DDCST:C_{60}, and PPT–CZ ($n=10$).

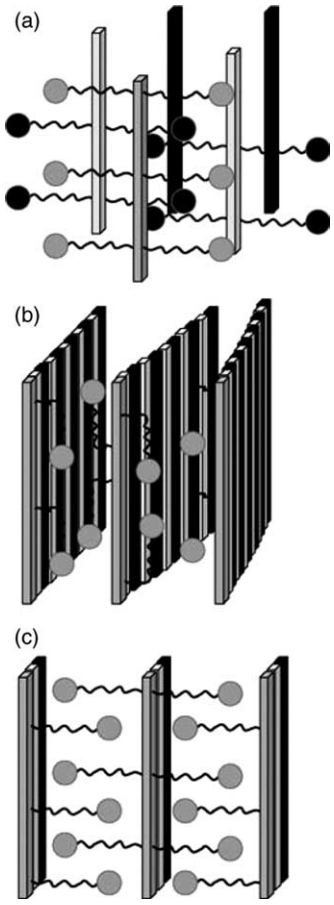

Fig. 4. Schematic illustrations of the mesophase structures: Proposed nematic-like mesophase for PPT–TPA (a) and (b) and the layered mesophase of PPT–CZ (c).

described above when discussing the absorption spectra. The second reason is related to the conformational structure of the photoconducting groups. In order to obtain a better insight into the conformational properties and steric demands of the side groups, optimized conformations of the analogues for PPP-CZ and PPT–TPA were calculated through Molecular Mechanics with Cerius 2 version 4.0 [33]. They were calculated by the model with the Universal force field (UFF) [34] and the DREIDING force field [35], which both leaded to similar results. The results by DREIDING force field are shown in Fig. 5. The bulky TPA groups of a propeller-shaped structure [36,37] are bent for 141° from the extended alkyl chain in TPA-CH_2O–$(CH_2)_{10}OCH_3$ (Fig. 5(b)), whereas the planar carbazole (CZ) group is parallel to the alkyl chain in CZ-$(CH_2)_{10}OCH_3$ (Fig. 5(a)). In the layered structure of PPT–CZ, the side-chains including the pendent carbazole group are in the linearly extended conformation as shown in Fig. 4(c). They are interdigitated with each other by a spacing of approximately 12 Å, which is a distance of the repeating unit of the PPT backbone [9]. However, in PPT–TPA the large size of the bulky TPA group ($\approx$11 Å) is too close to the distance between the interdigitated side-chains,

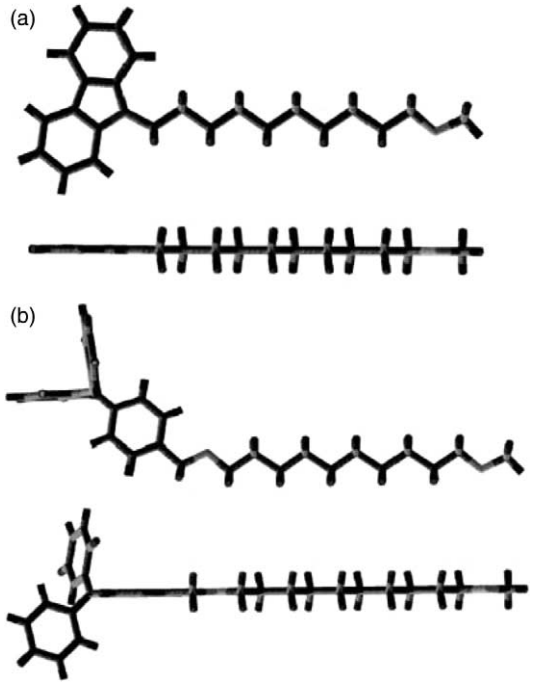

Fig. 5. Optimized geometry of the analogues (top and side views); (a) CZ-$(CH_2)_{10}OCH_3$, (b) TPA-CH_2O–$(CH_2)_{10}OCH_3$.

consequently a high steric hindrance occurs, which prevents the formation of the layered structure. Moreover, the bent conformation of TPA-CH_2O–$(CH_2)_{10}OCH_3$ can suppress the rotational freedom to form a linearly extended conformation due to a high rotational barrier in the limited volume between the interdigitated side-chains. Therefore, the PPT–TPA polymer is not likely to form an extended layered mesophase like PPT–CZ.

In the photorefractive composites PPT–TPA ($n=10$):DDCST:C_{60}, the mesophase structure and the layer distance do not change considerably as the photorefractive ingredients are mixed in contrast to PPT–CZ ($n=10$):DDCST:C_{60} where the layer thickness increases with respect to the host polymer PPT–CZ ($n=10$) [10]. Moreover, the photorefractive PPT–TPA ($n=10$) composites do not exhibit visible phase separation at least during our measurements and are of a very good optical quality, as also the case of PPT–CZ. Keeping this in view, we can expect a high local concentration of photorefractive active groups and strong orientational electro-optic effect in PPT–TPA composites as in the case of PPT–CZ composites described in Ref. [10].

3.5. Electro-optic and photoconductive properties

The electro-optical properties of the photorefractive composites were characterized by measuring the field-induced birefringence. As shown in Fig. 6, the change of the refractive index Δn increases with the applied electric field E as $\Delta n \approx RE^2$ with the Kerr constant $R=5.0\times10^{-7}$ $(V/\mu m)^{-2}$ for PPT–TPA ($n=10$):DDCST:C_{60}. Both

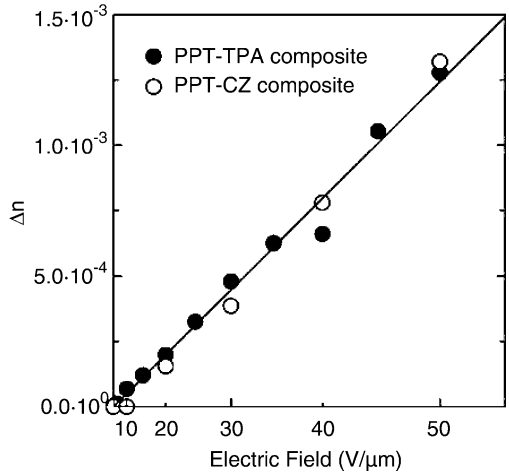

Fig. 6. Refractive index change Δn as a function of the applied electric field (on a quadratic scale) from the field-induced birefringence measurements; PPT–TPA ($n=10$):DDCST:C_{60} (filled circles), PPT–CZ ($n=10$): DDCST:C_{60} (open circles).

composites show the quadratic field dependence of Δn as expected for orientational nonlinearities in low T_g nonlinear optical polymers. From the electric-field induced phase shift $\Delta\phi=81.7°$ at $\lambda=633$ nm, $\cos\theta_{int}=0.89$, and $E=50$ V/μm we obtain $\Delta n=1.28\times10^{-3}$ for PPT–TPA ($n=10$):DDCST:C_{60}. The change of the refractive index Δn is given by $\Delta n=(n^3/2)r_{eff}E$ where n is the refractive index and r_{eff} the effective electro-optic coefficient. From the above parameters and $n=1.7$ we obtain $r_{eff}=10.4$ pm/V for $E=50$ V/μm. The resulting electro-optic coefficients for both composites are given in Table 1.

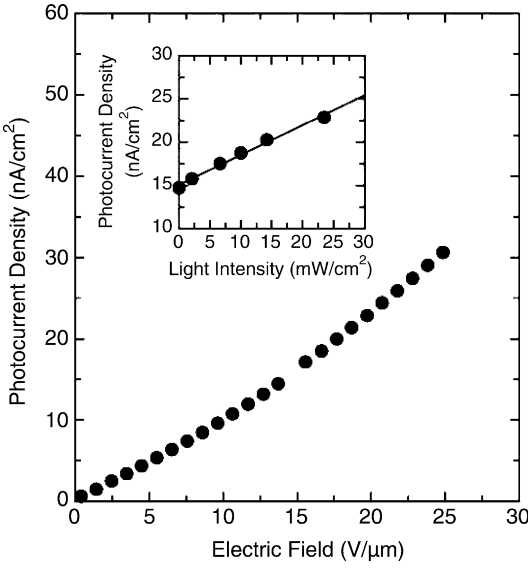

Fig. 7. Photocurrent densities of the photorefractive composite PPT–TPA ($n=10$):DDCST:C_{60} as a function of the external electric field at the light intensity of $I=23.5$ mW/cm^2 at $\lambda=633$ nm. The Inset shows the light intensity dependence of the photocurrent at the external electric field of $E=20$ V/μm.

Table 1
Absorption coefficient α (without considering reflections at the surfaces), dielectric constant ε, dark conductivity σ_{dark}, photoconductivity σ_{ph}, specific photoconductivity σ_{ph}/I, two-beam coupling gain coefficient Γ, diffraction efficiency η, grating formation time τ, specific response rate τ^{-1}/I, photorefractive sensitivity S_{n2} for the two investigated photorefractive polymer composites based on mesophase photoconductive polymers

Composite	α (cm^{-1})	ε	σ_{dark}[a] [$(10^{12}\,\Omega\,cm)^{-1}$]	σ_{ph}[a] [$(10^{12}\,\Omega\,cm)^{-1}$]	σ_{ph}/I[a] [$(10^{12}\,\Omega\,W\,cm)^{-1}$]	Γ[b] (cm^{-1})	η[b] (%)	τ[b] (s)	τ^{-1}/I^{b} s^{-1} $(W/cm^2)^{-1}$	S_{n2}[b] (cm^2/kJ)	r_{eff}[c] (pm/V)	
PPT–TPA ($n=10$): DDCST:C_{60}	54	3.2	0.075	0.04[d]	1.7	56	9.1	4.5[e]	4.0	2.0	10.4	This work
PPT–CZ ($n=10$): DDCST:C_{60}	37	3.9	0.024	0.17[f]	11.3	160	14.6	13[g]	2.3	1.3	10.7	[10]

[a] Taken at $E=20$ V/μm.
[b] $E=50$ V/μm.
[c] $E=50$ V/μm, $\theta_{ext}=50°$.
[d] $I=23.5$ mW/cm^2.
[e] $I=55.0$ mW/cm^2.
[f] $I=14.7$ mW/cm^2.
[g] $I=34.1$ mW/cm^2.

The photocurrent density increases with increasing electric field as shown in Fig. 7. We compared the dark conductivity σ_{dark} and photoconductivity σ_{ph} at an electric field of 20 V/μm (Table 1). The photoconductivity is here calculated from the difference of the current before and after illumination. The specific photoconductivity was extracted as σ_{ph}/I [38], according to the linear intensity dependence of the photocurrent in the inset of Fig. 7. The specific photoconductivity was about seven times lower in the new photorefractive composite based on PPT–TPA than in PPT–CZ composite (Table 1). The reasons for the lower photoconductivity of PPT–TPA composite are related to its different mesophase structure with a different degree of crystallinity. The biphasic morphology of our mesophases, either layered or nematic-like structure, complicates the interpretation of the nature of the charge transport process. It has been suggested that liquid crystal polymers like our samples consist of domains of the mesophase, which are separated by grain boundaries [2,3]. Accordingly, we may attribute the high photoconductivity to the proposition that crystalline regions favor charge transport just as dense three dimensional crystals do, whereas the phase boundaries act as traps resulting from a variation in the orientation and distance between the charge-transport sites and surrounding molecules [39]. The high mobility of photoconducting molecules inside the crystalline region suppresses static trapping. The trapping species are not clearly defined here but the total concentration of sites that can serve as traps certainly depend on the content of the disordered boundary region, thus varying in samples of different morphology. Keeping in mind this two-phase morphology, we reexamined closely the X-ray data previously obtained for the composites PPT–TPA and PPT–CZ containing the same chromophore DDCST. As follows from Fig. 3, PPT–TPA composite exhibits significantly more disordered regions than PPT–CZ composite. From the comparison of the relative area of the crystalline peaks to the liquid-like halo peak in our samples we estimated that the PPT–TPA composite contains about 40–50% less crystalline regions than the PPT–CZ composite. Moreover, the mesophase structure of PPT–TPA is less ordered than the layered mesophase of PPT–CZ as discussed before (Fig. 4). Thus we could suggest that the reason for the lower photoconductivity in the PPT–TPA composite is due to a higher concentration of charge traps than in PPT–CZ composite as a consequence of a different mesophase structure with a lower degree of crystallinity.

3.6. Photorefractive characterizations

The photorefractive properties of the composites PPT–TPA ($n=10$): DDCST:C_{60} were investigated by two beam coupling and Bragg diffraction experiments. Two-beam coupling is used to determine the photorefractive origin of the recorded gratings, and the latter technique provides information about the amplitudes of the space charge field

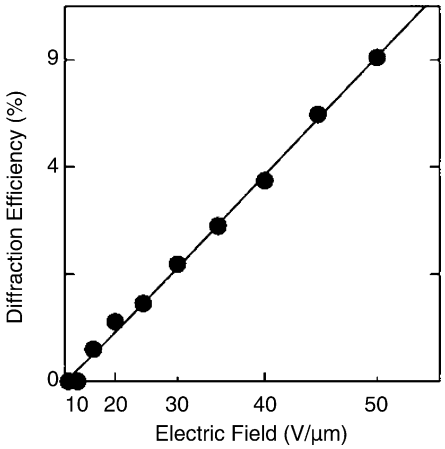

Fig. 8. Diffraction efficiency η on a square-root scale as a function of the external electric field (on a quadratic scale) for p-polarized writing beams at $\lambda = 633$ nm and p-polarized reading beam at $\lambda = 780$ nm.

and of the resulting refractive index modulation [24]. The two-beam coupling gain coefficient of our material was 56 cm^{-1} at $E = 50$ V/μm in the geometry described in the experimental part.

The dependence of the grating diffraction efficiencies on the applied field is shown in Fig. 8. The diffraction efficiency for the p-polarized read-out beam is much higher than for the s-polarized read-out beam with p-polarized writing beams [21]. The diffraction efficiency increases with increasing electric field. According to the coupled-wave theory [40], the solid line in Fig. 8 corresponds to the theoretical dependence $\eta = \sin^2(BE^2)$ with $B = 1.23 \times 10^{-4}$ $(V/\mu m)^{-2}$.

The grating formation time constant τ was obtained by using the relation,

$$\eta(t) = \sin^2\left\{A_0\left[1 - \exp\left(\frac{-t}{\tau}\right)\right]\right\}$$

assuming that the refractive index change has a single exponential time dependence. Fig. 9a shows the dynamics of the grating formation with a p-polarized read-out beam for the PPT–TPA composite at 50 V/μm, and a theoretical curve corresponding to the above equation with the response rate given in Table 1. The response rate increases with the electric field as shown in Fig. 9(b). We also determined the photorefractive sensitivity of the PPT–TPA composite and compared it with the PPT–CZ composite. The photorefractive sensitivity can be defined as the refractive index change per unit incident energy that is $S_{n2} = \partial(\Delta n)/\partial W_0$, where W_0 is the incident fluence of the optical energy per unit area [41,42]. We obtained S_{n2} value of 2.0 cm^2/kJ at applied field of 50 V/μm for a total incident intensity of 55 mW/cm^2.

In general, the photorefractive speed is limited by a photoconductivity-limited response if the orientational dymanics of NLO chromophores is much faster than the photorefractive dynamics. However, the photorefractive sensitivity of PPT–TPA ($n = 10$):DDCST:C_{60} is larger than

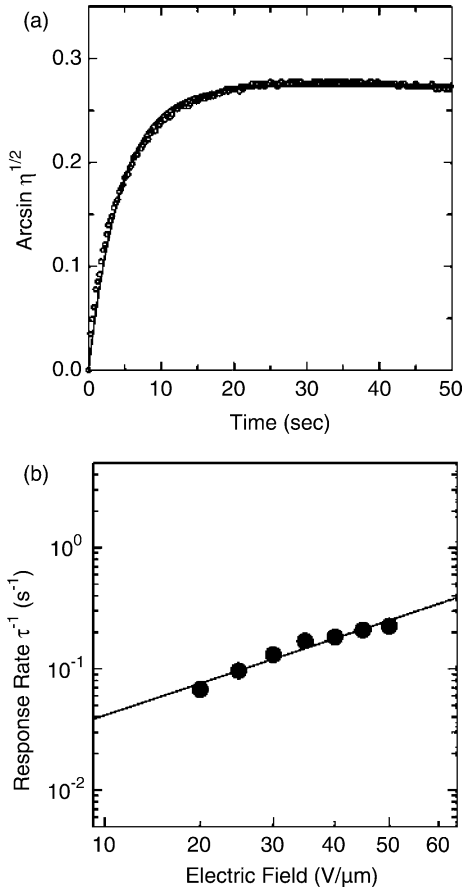

Fig. 9. (a) Buildup transient of the diffracted signal observed at $E = 50$ V/μm. (b) Response rate τ^{-1} as a function of the electric field (on a square-root scale) at $\lambda = 633$ nm with a total writing intensity of 55 mW/cm^2.

the one found in PPT–CZ ($n = 10$):DDCST:C_{60} for the same applied electric field, despite of the about seven times lower photoconductivity of the PPT–TPA composite, as shown in Table 1. The reason for this unexpected result can be related to the trapping characteristics of the two mesophase structures. As recently confirmed by Hofmann et al. [29], the photorefractive grating formation time is not only limited by the hole mobility but also by the trapping rate of the holes in the dark regions, which affects on the other side the dispersivity of charge transport. We could also suggest this in our preliminary experiments of the time-of-flight transient photocurrents. The photocurrent transient for the PPT–TPA polymer with a less ordered mesophase structure appears much more dispersive than for the PPT–CZ polymer with a highly ordered layered structure. A highly dispersive charge transport indicates a high concentration of traps [29]. This is in the case of PPT–TPA mostly due to a high concentration of phase boundaries in the suggested less-ordered mesophase structure. Therefore, the less-ordered mesophase structure of PPT–TPA decreases the photoconductivity on one hand, but increases the trapping rates on the other. This finally results in a faster photorefractive response and better sensitivity compared

to a layer structured PPT–CZ composite. A controlled engineering of the mesophase structure of photorefractive polymer composites should, therefore, present one of the possibilities to achieve the optimized photorefractive characteristics.

4. Conclusions

A new mesophase photoconductive polymer PPT–TPA has been synthesized. The polymer consists of wholly aromatic rigid backbone of poly(*p*-phenyleneterephthalate), PPT and pendent hole-transporting triphenylamine (TPA) groups that are attached at ends of oxydecyl spacers. PPT–TPA ($n=10$) exhibits a mesophase structure with an ordering between the nematic and the highly-ordered layer structure that is typical for the previously studied PPT–CZ polymer with a different charge transporting agent. The structural difference is a consequence of the bent conformation of bulky TPA groups in contrast to the linear conformation of the CZ group. The PPT–TPA composite without any plasticizer reveals the low value of the glass transition temperature near 15 °C, which classify this composite as a low-T_g material. Despite of the about seven times lower photoconductivity, the photorefractive composite PPT–TPA shows a higher photorefractive sensitivity S_{n2} of 2 ± 0.2 cm^2/kJ at $E=50$ V/μm than the previously studied PPT–CZ composite. The reasons could be related to a higher trap density associated with the different mesophase structure. This unexpected phenomenon will be the subject of future studies in order to exploit the high trapping ability of the new PPT–TPA photoconductive polymer.

Acknowledgements

This work was supported by Korea Research Foundation Grant (KRF-2003-042-D20044) and by the Swiss National Foundation (NF 2-777416-04).

References

[1] Ballauff M. Angew Chem Int Ed Engl 1989;28:253.
[2] Damman SB, Mercx FPM, Lemstra PJ. Polymer 1993;34:2726.
[3] Buijs JAHM, Damman SB. J Polym Sci, Polym Phys 1994;32:851.
[4] Watanabe JW, Harkness BR, Sone M, Ichimura H. Macromolecules 1994;27:507.
[5] Kricheldorf HR, Domschke A. Macromolecules 1996;29:1337.
[6] Sone M, Wada T, Harkness BR, Watanabe J, Takahashi H, Huang HW, et al. Macromolecules 1998;31:8865.
[7] Fu K, Nematsu T, Sone M, Itoh T, Hayakawa T, Ueda M, et al. Macromolecules 2000;33:8367.
[8] Heldmann C, Schulze M, Wegner G. Macromolecules 1996;29:4686.
[9] Lee ME, Seong SY, No KT, Kwon OP, Lee SH. Macromol Theory Simul 2004;13:265.
[10] Kwon OP, Lee SH, Montemezzani G, Günter P. Adv Funct Mater 2003;13:434.
[11] Kwon OP, Lee SH, Montemezzani G, Günter P. J Opt Soc Am B 2003;20:2307.
[12] Kwon OP, Montemezzani G, Günter P, Lee SH. Appl Phys Lett 2004; 84:43.
[13] Lee JW, Jin JI, Jo BW, Kim JS, Zin WC, Kang YS. Acta Polym 1999; 50:399.
[14] Lee SH, Kang YS, Song SJ. Chem Commun 1998;2513.
[15] Lee SH, Lee JW, Kwon OP, Lee CH, Won YH. Appl Phys Lett 1999; 74:2067.
[16] Kwon OP, Im JH, Kim JH, Lee SH. Macromolecules 2000;33:9310.
[17] Kwon OP, Cho DJ, Won YH, Lee SH. Macromolecules 2002;35: 4841.
[18] Ducharme S, Scott JC, Twieg RJ, Moerner WE. Phys Rev Lett 1991; 66:1846.
[19] Moerner WE, Grunnet-Jepsen A, Thompson CL. Annu Rev Mater Sci 1997;27:585.
[20] Meerholz K, Volodin BL, Sandalphon, Kippelen B, Peyghambarian N. Nature 1994;371:497.
[21] Moerner WE, Silence SM, Hache F, Bjorklund GC. J Opt Soc Am B 1994;11:320.
[22] Kippelen B, Sandalphon, Volodin BL, Meerholz K, Peyghambarian N. In: Jenkhe SA, Wynne KJ, editors. Photonic and optoelectronic polymers. Washington, DC: ACS; 1997. p. 218–35.
[23] Kippelen B, Meerholz K, Peyghambarian N. In: Nalwa HS, Miyata S, editors. Nonlinear optics of organic molecules and polymers. Boca Raton: CRC Press; 1997. p. 465–513.
[24] Günter P, Huignard JP. Photorefractive materials and their applications I and II. Berlin: Springer; 1988.
[25] Montemezzani G, Medrano C, Zgonik M, Günter P. In: Günter P, editor. Nonlinear optical effects and materials. Berlin: Springer; 2000. p. 301–73.
[26] Zhang Y, Wada T, Sasabe H. J Mater Chem 1998;8:809.
[27] Ostrauskaite J, Karickal HR, Leopold A, Haarer D, Thelakkat M. J Mater Chem 2002;12:58.
[28] Wright D, Gubler U, Moerner WE, DeClue MS, Siegel JS. J Phys Chem B 2003;107:4732.
[29] Hofmann U, Grasruck M, Leopold A, Schreiber A, Schloter S, Hohle C, et al. J Phys Chem B 2000;104:3887.
[30] Park SH, Ogino K, Sato H. Polym Adv Technol 2000;11:349.
[31] Higashi F, Hoshio H, Kiyoshige J. J Polym Sci, Polym Chem 1983;21: 3241.
[32] Ebert M, Herrmann-Schenherr O, Wendorf JH, Ringsdorf H, Tschirner P. Makromol Chem Rapid Commun 1988;9:451.
[33] Molecular Simulations Inc., 9685 Scranton Road, San Diego, CA 92121, USA.
[34] Rappe AK, Casewit CJ, Colwell KS, Goddard III WA, Skiff WM. J Am Chem Soc 1992;114:10024.
[35] Mayo SL, Olafson BD, Goddard III WA. J Phys Chem 1990;94:8897.
[36] Porres L, Mongin O, Katan C, Charlot M, Pons T, Metz J, et al. Org Lett 2004;6:47.
[37] Sancho-Garcia JC, Foden CL, Grizzi I, Greczynski G, De Jong MP, Salaneck WR, et al. J Phys Chem B 2004;108:5594.
[38] Zhao C, Park CK, Prasad PN, Zhang Y, Ghosal S, Burzynski R. Chem Mater 1995;7:1237.
[39] Adam D, Schuhmacher P, Simmer J, Haussling L, Siemensmeyer K, Etzbach KH, et al. Nature 1994;371:141.
[40] Kogelnik H. Bell Syst Tech 1969;48:2909.
[41] Günter P. Phys Rep 1982;93:199.
[42] Montemezzani G, Günter P. In: Keller O, editor. Notations and perspectives of nonlinear optics. Singapore: World Scientific; 1995. p. 370–427.